JOURNAL OF MATERIALS SCIENCE 28 (1993) 4787–4798

A quantitative evaluation of microstructure in Si_3N_4/SiC platelet and particulate composites

G. PEZZOTTI
The Institute of Scientific and Industrial Research, Osaka University, Ibaraki 567 Osaka, Japan

B.-T. LEE, K. HIRAGA
Institute for Materials Research, Tohoku University, Katahira, Aoba-ku, Sendai 980, Japan

T. NISHIDA
Kyoto Institute of Technology, Faculty of Polytechnique Science, Department of Materials Engineering, Matsugasaki, Sakyo-ku, Kyoto 606, Japan

A microstructural evaluation of Si_3N_4 containing 15–40 vol % SiC platelets or particles is presented. All the composites were fully densified by hot isostatic pressing without external addition of sintering aids. Size, morphology, surface roughness and crystal structures of the SiC phases before and after sintering were compared in order to discuss the structural stability of the reinforcements up to 2050 °C in Si_3N_4 matrix. Morphology and phase characteristics of the grain boundary are also discussed. In addition, homogeneity and isotropy of the composite bodies were quantitatively examined by image analysis techniques and it was recognized that, for a similar degree of dispersion, the characteristic of three-dimensional randomness could be preserved only at $V_f < 30\%$ in the composites containing high aspect ratio platelets.

1. Introduction

In many fracture situations, the quantitative evaluation of microstructural parameters holds a remarkable position in linking idealized fracture mechanics models with experimental studies of fracture behaviour. The rigorous experimental determination of spatial geometrical parameters characterizing grain size, shape, distribution and orientation of the constituent phases of a composite material, for example, constitutes a decisive step in relating the operative microfracture mechanisms to the macroscopic measurements of fracture resistance. The statistically exact relationships of stereology dealing with areal, lineal and feature-count analyses, locate the appropriate parameters and provide the mathematical basis for such evaluation.

In addition to the geometry of the composite microstructure, however, other important microstructural circumstances must be investigated together in order to give a rationale of the mechanical behaviour of a composite material. They lie on the atomic scale and are related to the crystal structure and the interface characteristics of the microstructural features.

In this work a comprehensive evaluation of microstructure was attempted by comparing two Si_3N_4/SiC composites fabricated by the same processing method and containing 15–40 vol % two different SiC raw powders with similar average particle size. These materials have recently received attention as possible candidates for gas turbine engines because of their high refractoriness up to 1400 °C [1–3]. Both geometric parameters and crystal structures, as well as the phase characteristics of the grain boundary, were taken into consideration in the present study. Techniques were mainly electron and X-ray diffraction analysis (XRD), optical (OM), scanning electron (SEM) and transmission electron microscopy (TEM), followed by quantitative image analysis. The purity of the constituent phases was investigated by chemical analyses. Based on electron diffraction analyses results, the influence of a sintering temperature as high as 2050 °C on the structural stability of the SiC phase was examined and discussed. This basic investigation represents the starting point for a detailed analysis of fracture behaviour which will be presented in a forthcoming report [4].

2. Materials and processing

2.1. Characterization of starting powders

Commercially available pure Si_3N_4 (E-10, Ube Ind., Ube, Japan) and two different SiC raw powders denoted powders A (Grade M, c-Axis Technology, Jonquiere, Canada) and B (GC 600, Showa Denko, Nagano Prefecture, Japan) were used. Table I shows the results of impurity analysis obtained using an inductively coupled radio-frequency plasma emission spectrometer (ICP) after dissolving the starting powders in HF at 25 °C. The SiC powders were treated at 1000 °C in a mixture of Na_2CO_3 and H_2BO_3 prior to

0022–2461

ICP analyses. It is clear that in the composite bodies, the impurity contained in the SiC phases will contaminate the highly pure Si_3N_4 material. In particular, the SiC powder A contained a higher percentage of aluminium. Some of these impurities may lead to a detrimental effect on the high-temperature properties of the composite [3].

X-ray diffraction analysis with CuK_α radiation were performed for the two SiC starting powders in the range 10°–80° 2θ with scanning at 1° min^{-1}. To minimize the effect of preferred orientation, the SiC powders were previously finely crushed in a tungsten carbide mortar and then compacted in a concave glass sheet for measurement. The results of these experiments (shown in Fig. 1 for the angle range of interest) indicated that both the powders were mainly constituted by two SiC polytypes: 4H and 6H. A precise quantitative determination of the amount of these polytypes, however, was not possible in this study because of the superposition of the major peaks. Peak breadth and the presence of many satellite peaks indicated the high density of stacking faults existing in both the SiC powders. A minor amount of the polytype 15R was also observed in both the powders, as revealed by the two weak peaks detected at 37.6° and 38.6° (cf. Fig. 1). Neglecting the presence of the polytype 15R and other undetected species, we roughly estimated the presence of about 45 wt % 4H and 55 wt % 6H in Powder A while Powder B was found to mainly consist of the polytype 6H (95 wt %).

Low-magnification SEM images of the raw SiC Powders A and B are shown in Fig. 2a and c respectively, together with their particle-size distributions (Fig. 2b and d). Particle-size analyses were conducted by the laser-transparency method after suspension in ethylene glycol. The two SiC powders had both a narrow particle-size distribution with an average size of 24 and 28 μm, respectively. Despite their similar mean size and shape by low-magnification observation, however, Powders A and B showed marked geometrical differences after a more detailed characterization. High-magnification SEM better revealed both higher shape irregularity and surface roughness in Powder B (Fig. 3b) compared with Powder A (Fig. 3a). They are obviously related to the grinding process adopted to reduce Powder B to the desired size. A precise characterization of size and morphology was better performed once the SiC powders were embedded in the Si_3N_4 matrix by adopting image analysis techniques. The results of these characterizations will be presented in Section 3.

Specimens of both the SiC powders were examined by TEM after crushing the as-received powders to sub-micrometre size and placing them on a carbon film. Thin SiC flakes were viewed normal to their [0 0 0 1] axis. In addition, analysis by TEM indicated

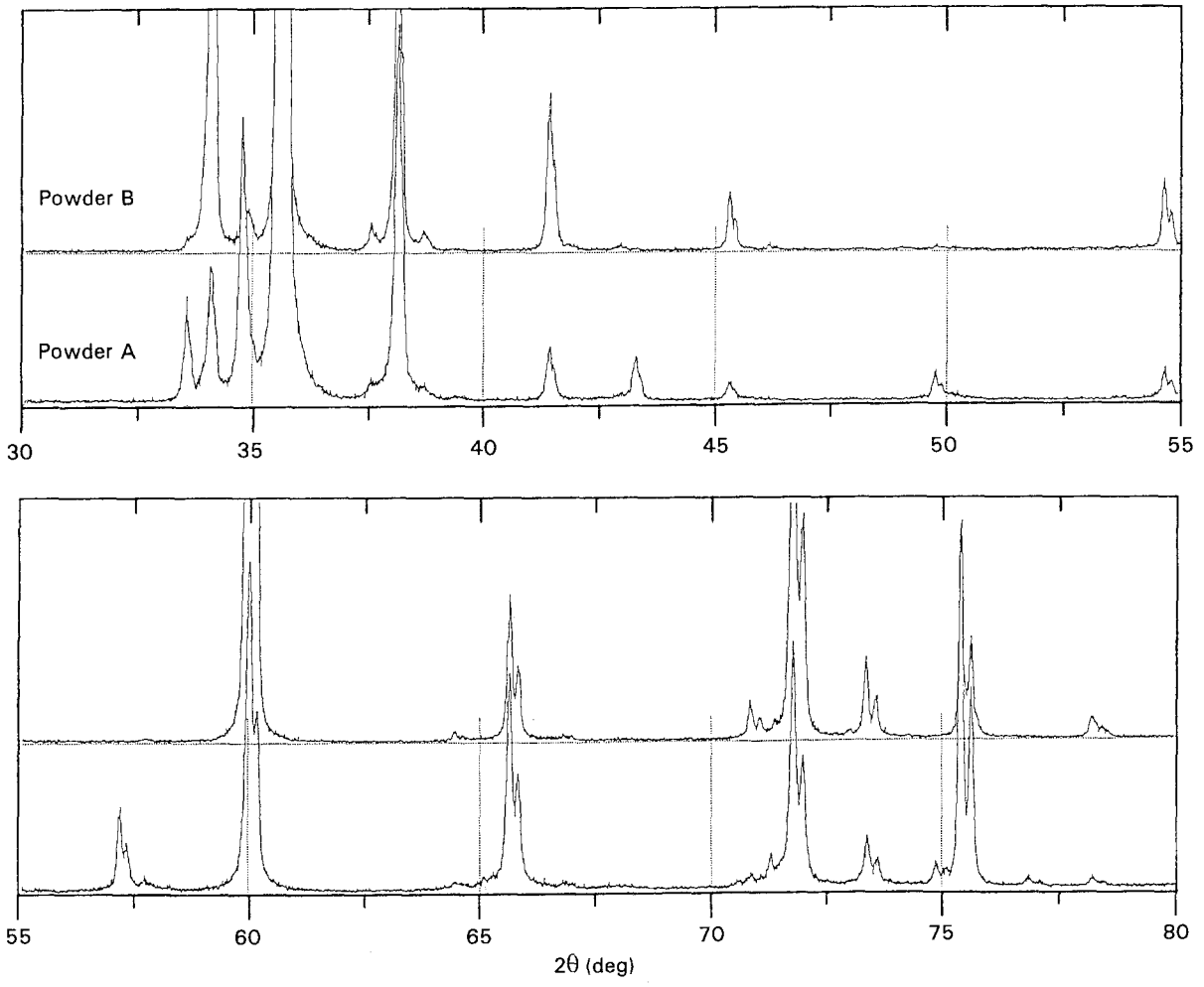

Figure 1 XRD patterns of starting SiC Powders A and B.

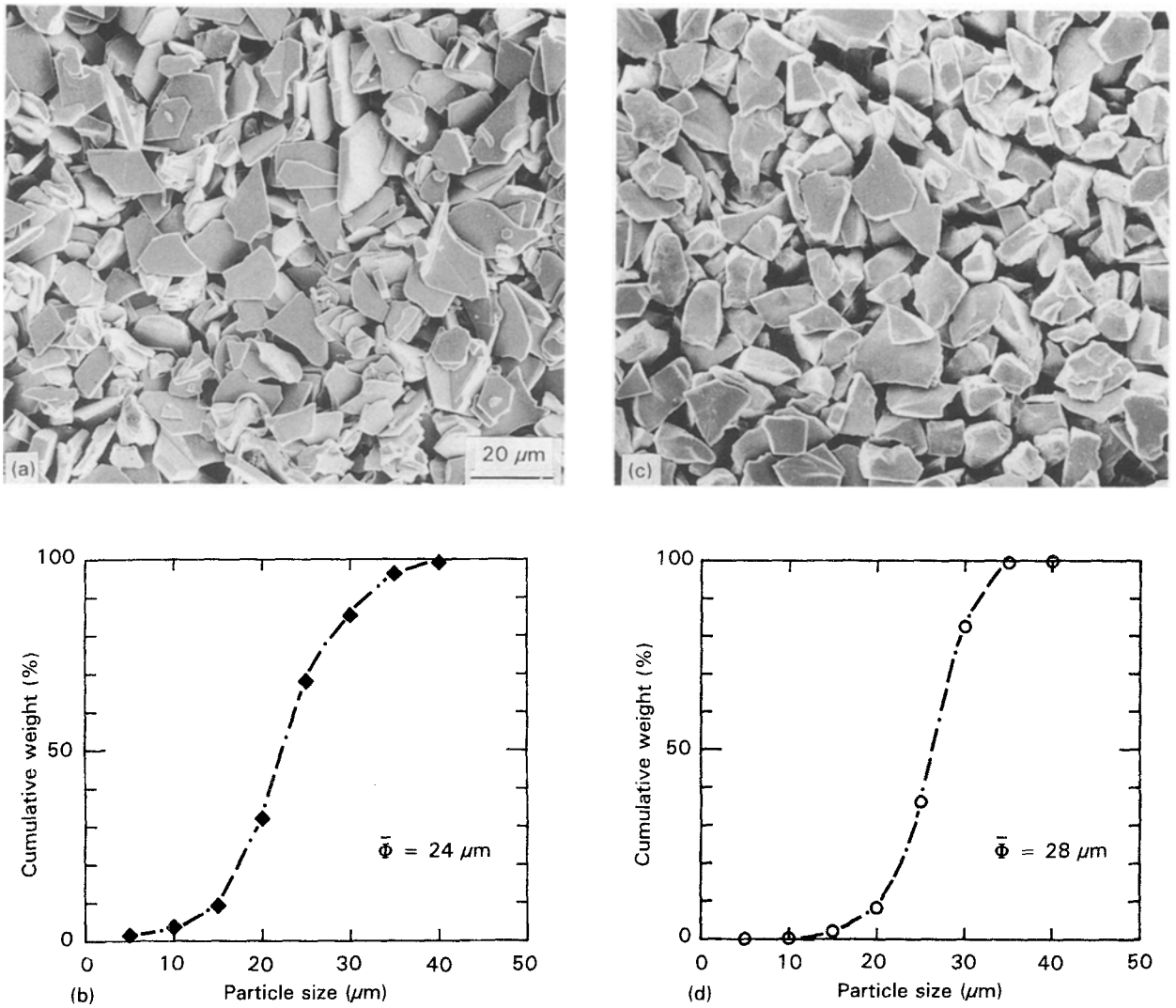

Figure 2 Low-magnification SEM images of the starting SiC Powders (a) A and (c) B with (b, d) their respective particle-size distributions.

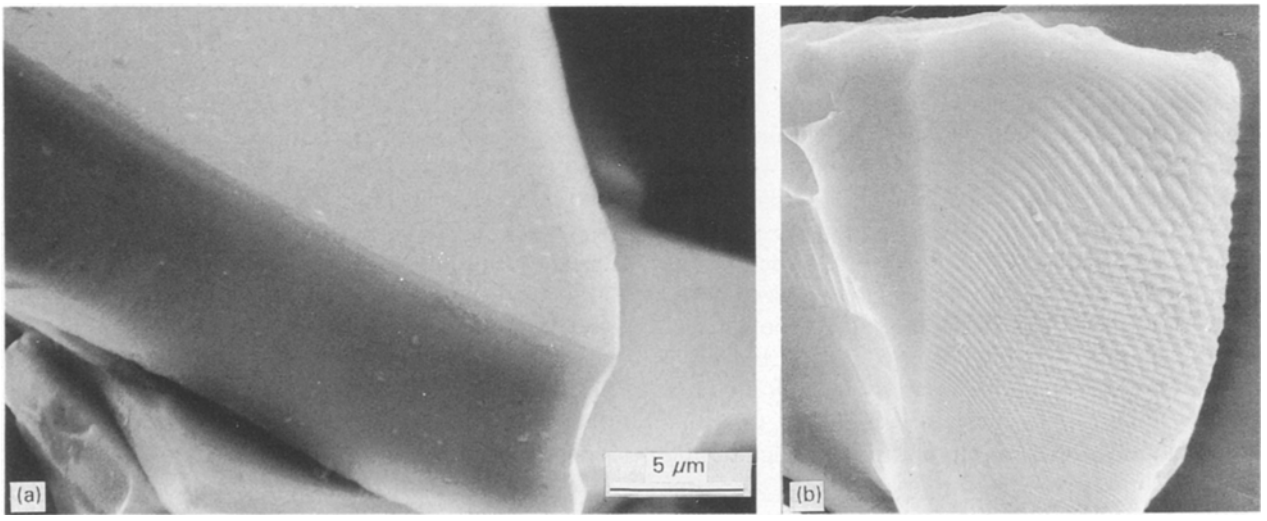

Figure 3 High-magnification SEM images showing surface characteristics of the starting SiC Powders (a) A and (b) B.

percentages of polytypes similar to that found by XRD, although only a limited number of SiC flakes could be studied in detail. We found mainly polytype 6H in Powder B, and six flakes of the ten examined overall were primarily 4H in Powder A. Both the powders contained a significant density of stacking faults and microtwins. No obvious differences between the two starting powders could be found. Defect-free regions were also observed. The overall dimension of these latter regions will be better characterized by

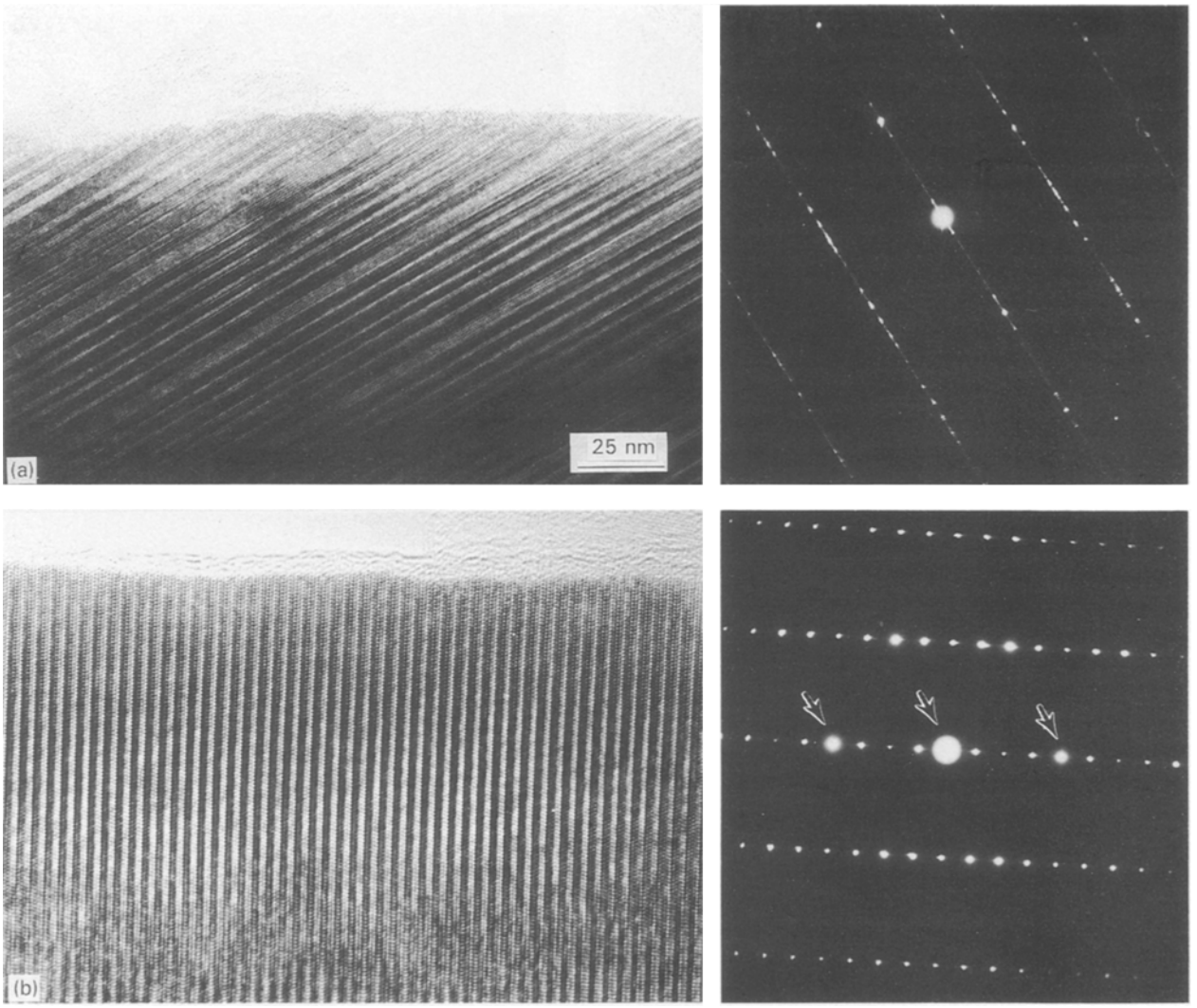

Figure 4 High-resolution TEM images of (a) a faulted and (b) an unfaulted region found in the starting SiC Powder A with the respective diffraction patterns.

observing the TEM specimens prepared from the sintered bodies in which the observable (thin) regions of the SiC-phase were larger (see Section 4). Fig. 4a and b show the high-resolution TEM images of a faulted and an unfaulted SiC region, respectively, found in two different SiC flakes of Powder A. The unfaulted flake (Fig. 4b) was easily recognized as 4H polytype from the repeat distance of the spots (measured as about 1 nm) and from the fact that every fourth diffraction spot (arrowed in Fig. 4) in each row is more intense than the other spots. On the other hand, the diffraction pattern of the defect-rich sample (Fig. 4a) showed very closely spaced spots along the [0 0 0 1] direction and a continuous streaking, indicating that the stacking faults observed in this zone are not perfectly regular in spacing. The main crystal structure of this SiC flake was 6H. However, small zones of different polytypes seem to exist as various substructures originated by the stacking faults sequence. These substructures are not easily recognized due to the continuous presence of streaks. Among them, the polytype 15R which was also detected by XRD, may be rather common.

2.2. Fabrication of composites

A wet procedure using a rotary evaporator immersed into an ultrasonic bath, was followed to mix matrix and reinforcement raw powders. The mixing medium was ethanol. Plastic-coated steel balls were also introduced during the wet mixing in order to promote an intimate dispersion of the SiC reinforcement inside the matrix. SEM observation of the mixtures indicated that almost no breakage of SiC occurred. This observation will be later quantitatively confirmed by image analysis. Five "green" specimens of two kinds of composites were obtained by dispersing 15–40 vol % SiC Powders A and B, respectively. A preforming cycle was performed by cold isostatic pressing (CIP) at 200 MPa. The preformed specimens were then coated with BN powder by a further CIP cycle, prefired *in vacuo* at 1200 °C and encapsulated in evacuated borosilicate glass. Then, HIP sintering at 2050 °C for 1 h under 180 MPa was performed to produce fully densified specimens (density > 99.5% by Archimedes' immersion method). Composite sintered bodies containing SiC Powders A and B, are hereafter simply denominated Composites A and B.

3. Image analysis

3.1. Morphology and dispersion of the SiC reinforcements

The microstructures of Composites A and B were observed both on OM and SEM scale after surface polishing. Before SEM observation, the polished surfaces were also etched in molten NaOH at 380 °C for 60 s. This procedure also allowed observation of the matrix microstructure. Fig. 5 shows the results of this experiment for the materials containing 25 vol % SiC. As seen in Fig. 5a and c, the section shapes of the SiC phase in Composites A and B appear to be quite different. The higher surface roughness of Powder B also seems to originate an interlocked Si_3N_4/SiC boundary compared with the smooth contours seen in Composite B. This fact may play an important role in the fracture behaviour of these two materials. On the other hand, the grain size and morphology of the Si_3N_4 matrix were approximately the same in both composites, as seen by comparing Fig. 5b and d. The Si_3N_4 grains were almost equiaxed. Their average grain size, accurately measured by superimposing several circles on to the micrographs [5], was in the range 1–2 μm for all the composites investigated. Generally, additions > 20 vol % SiC retarded the growth of the matrix grains during sintering. In fact, the grain size of the composites was almost the same as that of monolithic Si_3N_4 sintered at temperatures about 100 °C lower, according to a similar HIP schedule [6]. However, some exceptionally large and acicular Si_3N_4 grains (10–20 μm) was sporadically observed in Composite A. This phenomenon is thought to be due to the concurrent effect of the high sintering temperature and the local presence of impurities in the SiC phase because such large grains were always observed in the close neighbourhood of the SiC phase, and they were not found in the monolithic material [6].

Shape, size and dispersion of the SiC phase were quantitatively evaluated by analysing OM images. The specification of the mean shapes of SiC was first attempted by counting the number of edges on planes of polish, randomly cut through the composite specimens. The frequency of the number of edges as determined after sintering for Powders A and B, is shown in Fig. 6. The shape of the SiC Powder B was found to be closer to that of randomly distributed cubes (also shown in Fig. 6) rather than to other regular polyhedrons [7]. The histogram of Powder A was very close to the monovalue distribution of a thin disc or polygonal prism geometry. Histograms for the observed length, H_{obs}, and thickness, t_{obs}, of the SiC phase were also determined (Fig. 7). In the case of Powder A, lengths (defined as the major dimension) and thicknesses (length perpendicular to the major dimension) of the planar sections were easy to distinguish being generally $H_{obs} \gg t_{obs}$. The narrow distribution of thicknesses and the high symmetry of the length histogram support the assertion of a thin mean shape of Powder A. On the other hand, Powder B showed very similar histograms of H_{obs} and t_{obs} or, in

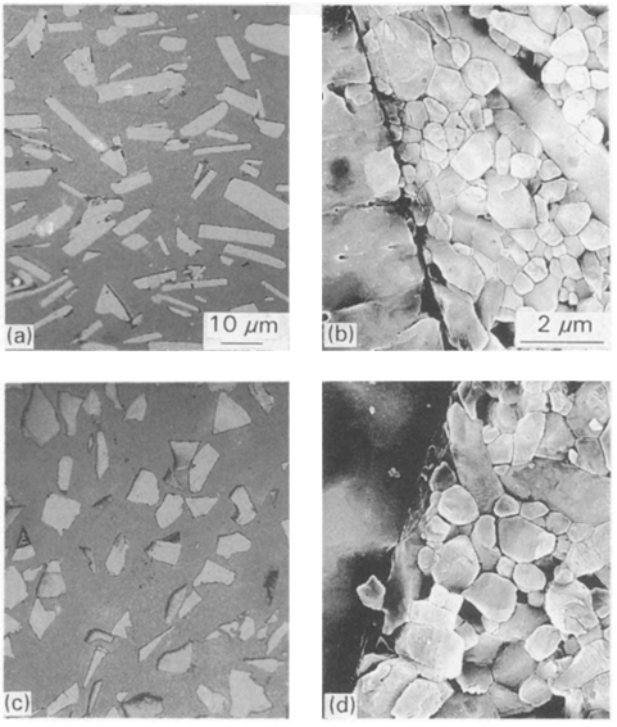

Figure 5 OM images of polished surfaces and respective SEM images after chemical etching of Si_3N_4/25 vol % SiC Composites (a, b) A and (c, d) B.

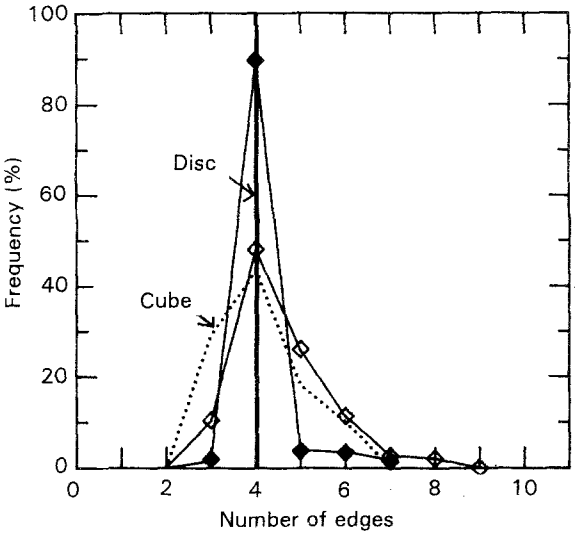

Figure 6 Histograms of the number of edges of the SiC phases measured on random sections compared with literature data for regular shapes [7]. (◆) Platelets, (◇) particles.

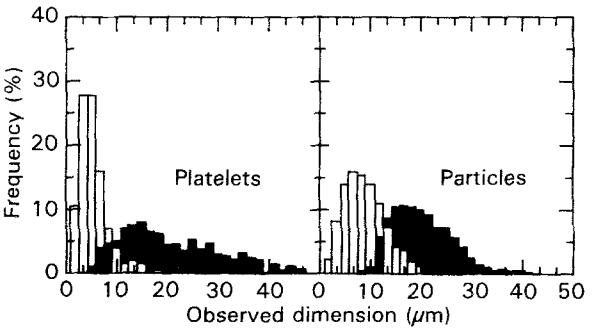

Figure 7 Histograms of the observed (■) length and (□) thickness of the SiC phases measured on random sections for Composites A and B.

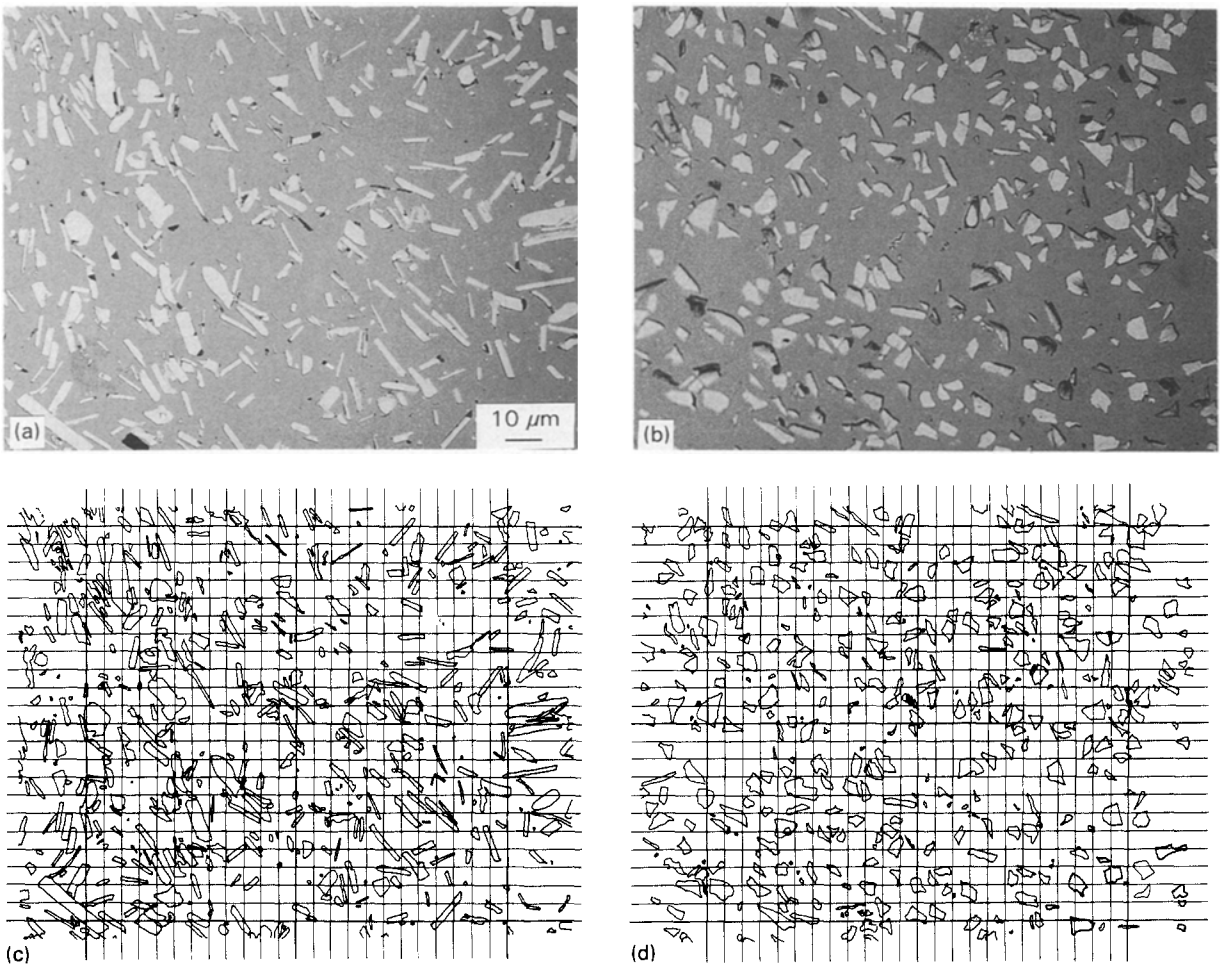

Figure 8 Scanning electron micrographs of platelet and particulate composites analysed by a random square grid.

other words, an aspect ratio, R, close to 1. Based on this analysis, the SiC phase of Composites A and B will be referred to as SiC platelets and particles, respectively, the main shape of the former being considered in first approximation as a thin disc, and that of the latter as a cube.

A procedure for determining the "true" dimensions from quantities measured on a two-dimensional plane of polish, has been suggested by Fullman [8] for a number of regular shapes using a probabilistic approach and basic stereological equations. The results of the analysis for circular plates are valid under the hypotheses of thin features and random sampling. According to Fullman's theory and assimilating the SiC phase of the present Composite A to thin discs, the average true diameter, $\bar{H}_{tr}$, and true thickness, $\bar{t}_{tr}$, were calculated from the histograms of Fig. 7 using the following equations

$$\bar{H}_{tr} = \pi/4Q \quad (1)$$

$$\bar{t}_{tr} = \pi S/4Q \quad (2)$$

where Q is the average value of the inverse of the observed diameter, H_{obs}, and S is the average value of the ratio of the observed thickness, t_{obs}, to H_{obs}. According to these calculations, an average thickness and an average diameter of 3.2 and 26.2 μm, respectively, were found for the SiC platelets embedded in Composite A. They result in an average true aspect ratio $\bar{R}_{tr} = \bar{H}_{tr}/\bar{t}_{tr} = 8.2$.

The average intercept length, $\bar{L}$, and centre-to-centre neighbouring distance, $\bar{\Delta}$, of the SiC-phases contained in Composites A and B were determined by lineal analysis, where the term "lineal" refers to an

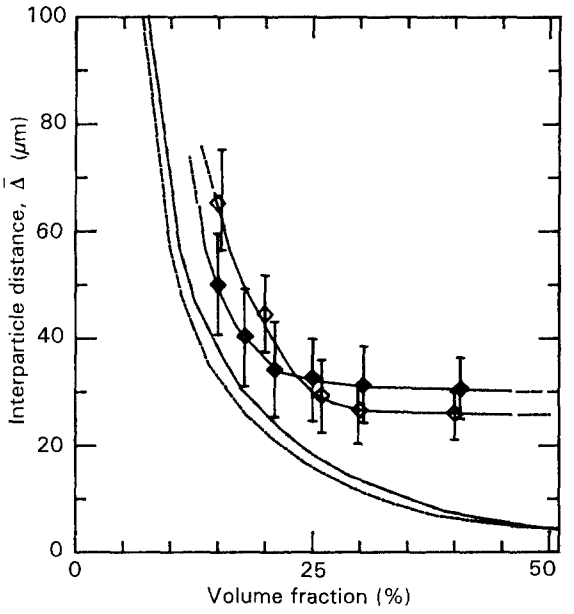

Figure 9 Dependence of the average centre-to-centre distance, $\bar{\Delta}$, and its relative standard deviation upon the volume fraction of the SiC phase, V_f, as measured by lineal analysis in Composites A and B. Comparison is made with theoretical dependences calculated for regular monodispersed shapes ([9] p. 83). (◆) Platelets, (◇) particles, (– – –) theoretical disc, (——) theoretical cube.

array of straight lines randomly superimposed on the micrographs. Fig. 8a and b show typical OM images which were enlarged, transformed into binary images and analysed under a random grid (Fig. 8c and d). The measured $\bar{L}$ values of SiC platelets and particles were 7.0 ± 3.4 and 8.2 ± 5.5 μm, respectively. The value of the mean edge length of the SiC particles when assimilated to regular monodispersed cubes, is obtainable from the measured $\bar{L}$ value by means of basic stereological equations ([9] p. 92). This is found to be

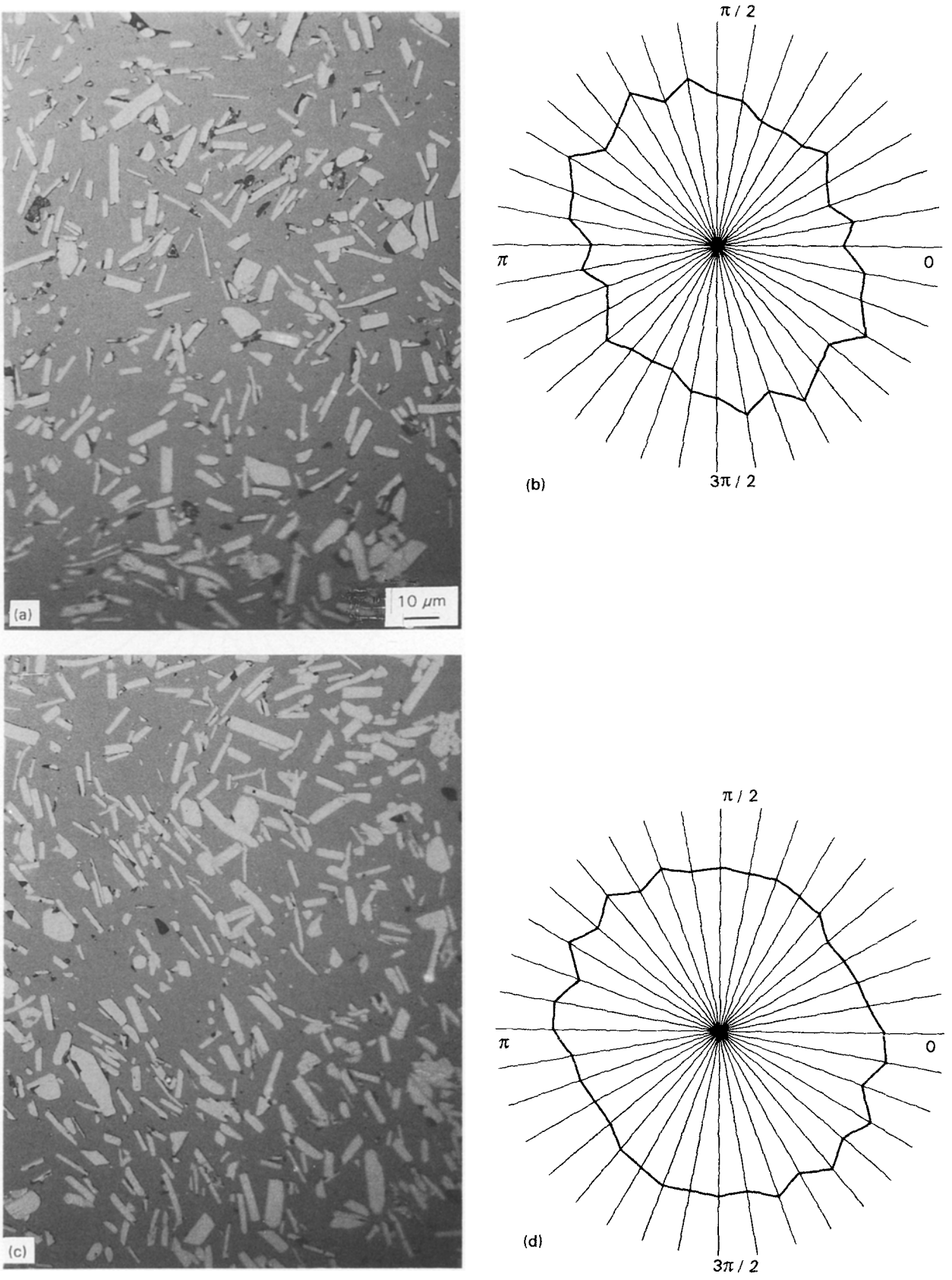

Figure 10 Optical micrographs and relative polar plots of the number of interceptions per unit length as found in two reciprocally perpendicular planes randomly cut through the sintered body of Composite A containing 20 vol % SiC phase.

$a = 3\bar{L}/2 = 12.3$ μm. Average values and relative standard deviations of the centre-to-centre neighbouring distance, $\bar{\Delta}$, are plotted for Composites A and B in Fig. 9 as a function of volume fraction, V_f. The abscissa of this plot represent the volume fractions as measured over the total investigated area which were, obviously, slightly different from the nominal additions of SiC. The volume fraction of each specimen was determined by systematic point counting [10] using the same random grid shown in Fig. 8 and counting the points falling exactly on the Si_3N_4/SiC boundary as one-half [11]. In Fig. 9, experimental data are compared with the theoretical dependences of V_f calculated from the L values for randomly oriented monodispersed discs and cubes, respectively. The following basic equation was used in the theoretical computation ([9] p. 83)

$$\bar{\Delta} = \bar{L}\,[(1 - V_f)^2/V_f] \quad (3)$$

where $\bar{L}$ is equal to $2t_{tr}$ and $2a/3$ in the case of discs and cubes, respectively. Comparing data for Composites A and B, it can be pointed out that no significant statistical difference seems to exist between the $\bar{\Delta}$ values of these two materials for fractions larger than 20 vol % this being the difference between the two experimental curves within the respective data scattering. A more definite difference appears to be at low fractions of SiC (< 20 vol %). It is difficult, however, to interpret whether such a difference is due to the different morphology of the SiC phases or to a different degree of homogeneity of the two composites. Generally, it was found that at $V_f < 20\%$ the experimental curves were almost constantly shifted to higher values with respect to the theoretical ones and, for $V_f > 20\%$, this difference tended towards an increase with increasing V_f. In addition to statistical factors such as the non-uniformity of particle size and morphology or the technological difficulty of uniformly dispersing high aspect ratio particles in the matrix, it should be considered that the theoretical curves in Fig. 9 are obtained under the hypothesis of a three-dimensionally random arrangement of the SiC phase. As shown in detail in the next section, however, such a hypothesis cannot be preserved at high V_f, owing to the impenetrability of real particles.

3.2. Orientation of the SiC reinforcing phases

It is well known that preferential orientations of the reinforcing phase can significantly affect the fracture behaviour of the composite, leading to a marked anisotropy of properties. In the present study, we attempted to address quantitatively the degree of orientation for increasing V_f of the SiC phase. It should be emphasized first that, although an isostatic pressing method was used to process the present composites, the presence of preferential orientation cannot be excluded a priori. During packing/sintering of real composites, in fact, even by isostatic pressing, local factors such as agglomerates, surface roughness and high aspect ratios of the added phase can be responsible for a non-random dispersion inside the matrix.

A polar plot of the number of interceptions per unit length of test line, P_1, [12] was constructed by superimposing on optical micrographs of the composite polished surfaces, a test array of lines placed at constant angular increments of 10°. Fig. 10a and c show

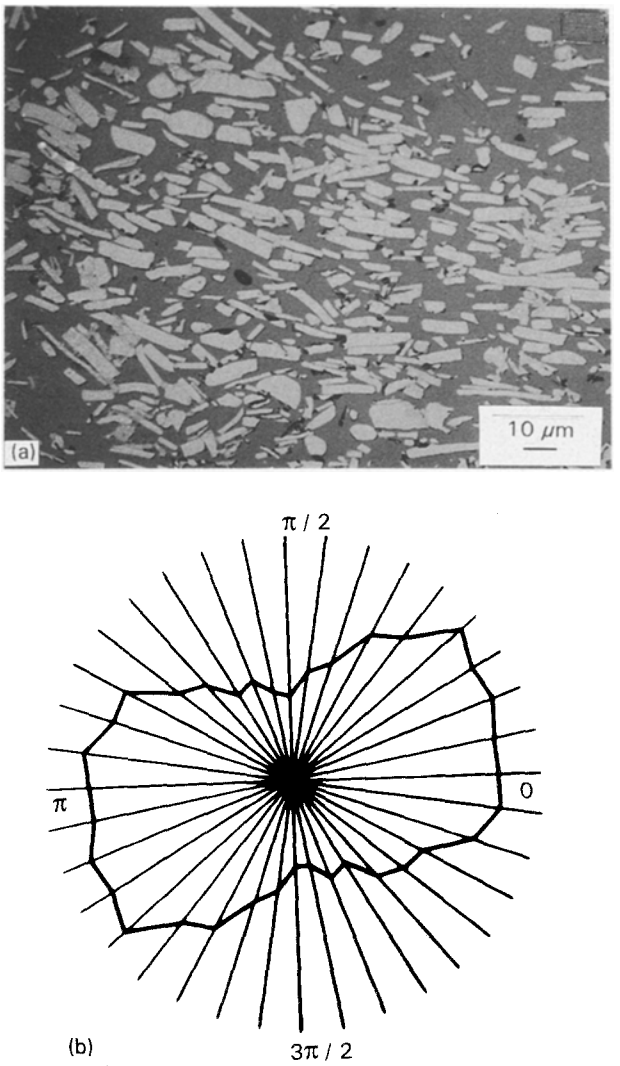

Figure 11 Local alignment of SiC platelets and relative degree of orientation in Composite A containing 40 vol % SiC phase.

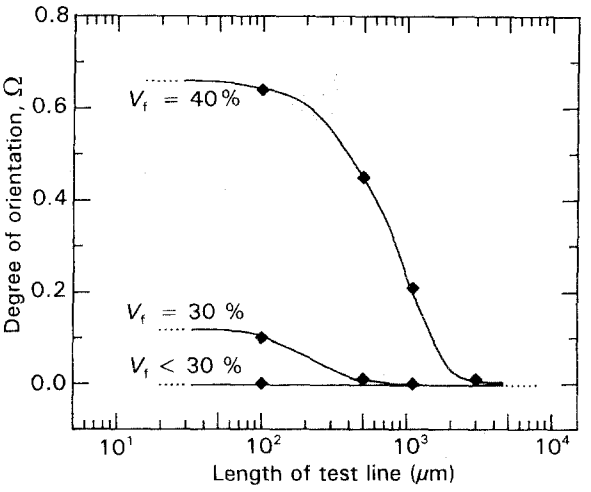

Figure 12 Dependence of the degree of orientation, Ω, upon the length of test line for Composite A containing various fractions of SiC phase.

typical OM microstructural images taken on two perpendicular planes inside Composite A with 20 vol % platelets. The polar plots constructed over these two photos are also shown in Fig. 10b and d. Similar to the results shown in Fig. 10, the polar plots for composites containing $V_f < 25\%$ platelets were always found to be very close to circles, whatever the investigated plane. These results prove the high degree of randomness obtained by HIP in composites containing low fractions of SiC phase. On the other hand, at $V_f > 30\%$ marked local anisotropy was observed in the platelet composites. In other words, in these composites, the shape of the polar plot depended upon the length of the test line. When the length of the test line was < 0.1 mm, as in the case of Fig. 11 (the same length as that adopted in the measurements of Fig. 10), partially asymmetric "roses" revealed local alignments along one preferential axis. This local anisotropy, however, was found to be independent of the orientation of the sampling plane, and the direction of the local orientation axis was detected to be random inside each single sampling plane. In partially oriented systems with one orientation axis, the degree of orientation, Ω, is defined as ([9] p. 58)

$$\Omega = [(P_1)_\perp - (P_1)_{||}]/[(P_1)_\perp) + 0.571\,(P_1)_{||}] \quad (4)$$

where Ω can vary between 0 and 1 and the experimental parameters $(P_1)_{||}$ and $(P_1)_\perp$ represent the number of interceptions per unit length in the directions parallel and perpendicular to the orientation axis, respectively. Fig. 12 summarizes the dependence of Ω on the length of test line, L_c, for different V_f of SiC platelets in the Composite A. As seen, the dimension characteristic of the local anisotropy in Composite A was in the range 0.5–2 mm for $V_f < 30\%$ while the composites containing platelet fractions < 30 vol % had high degree of three-dimensional randomness whatever the scale of observation. From a phenomenological point of view, it is clear that, in the range between 30 and 40 vol % for $R \sim 8$ (Fig. 11), when $\bar{\Delta}$ approaches very closely to H_{obs}, a random arrangement cannot be preserved because of the impenetrability of the SiC phase and partial alignment must occur. For high added fractions of a high aspect ratio phase, therefore, care must be taken in considering the composite as isotropic, depending upon the scale of the phenomenon under investigation.

4. Interfaces and crystal structures after sintering

Detailed information about the composite microstructures after HIP sintering were obtained by TEM. Samples for the TEM experiments were cut into thin

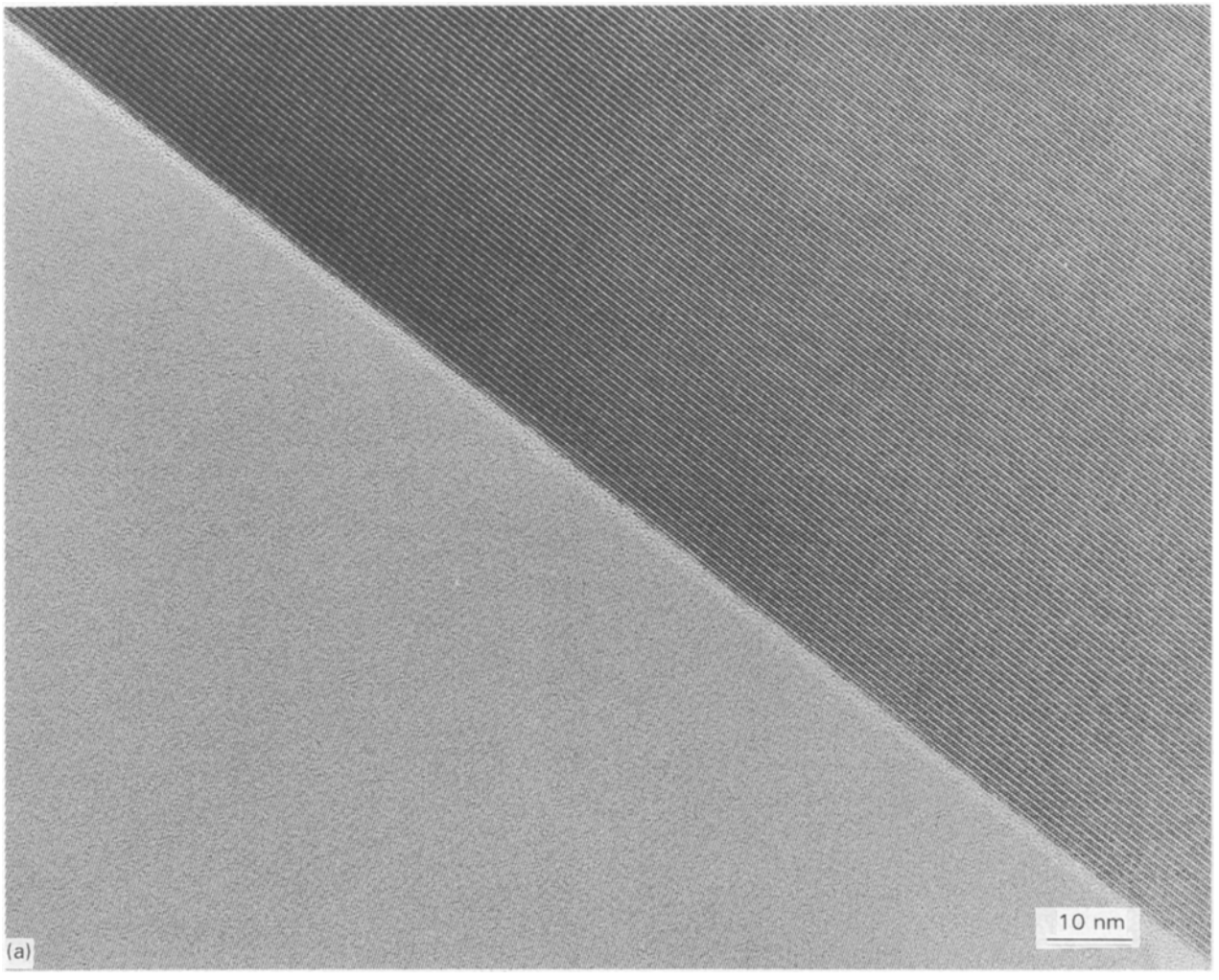

Figure 13(a)

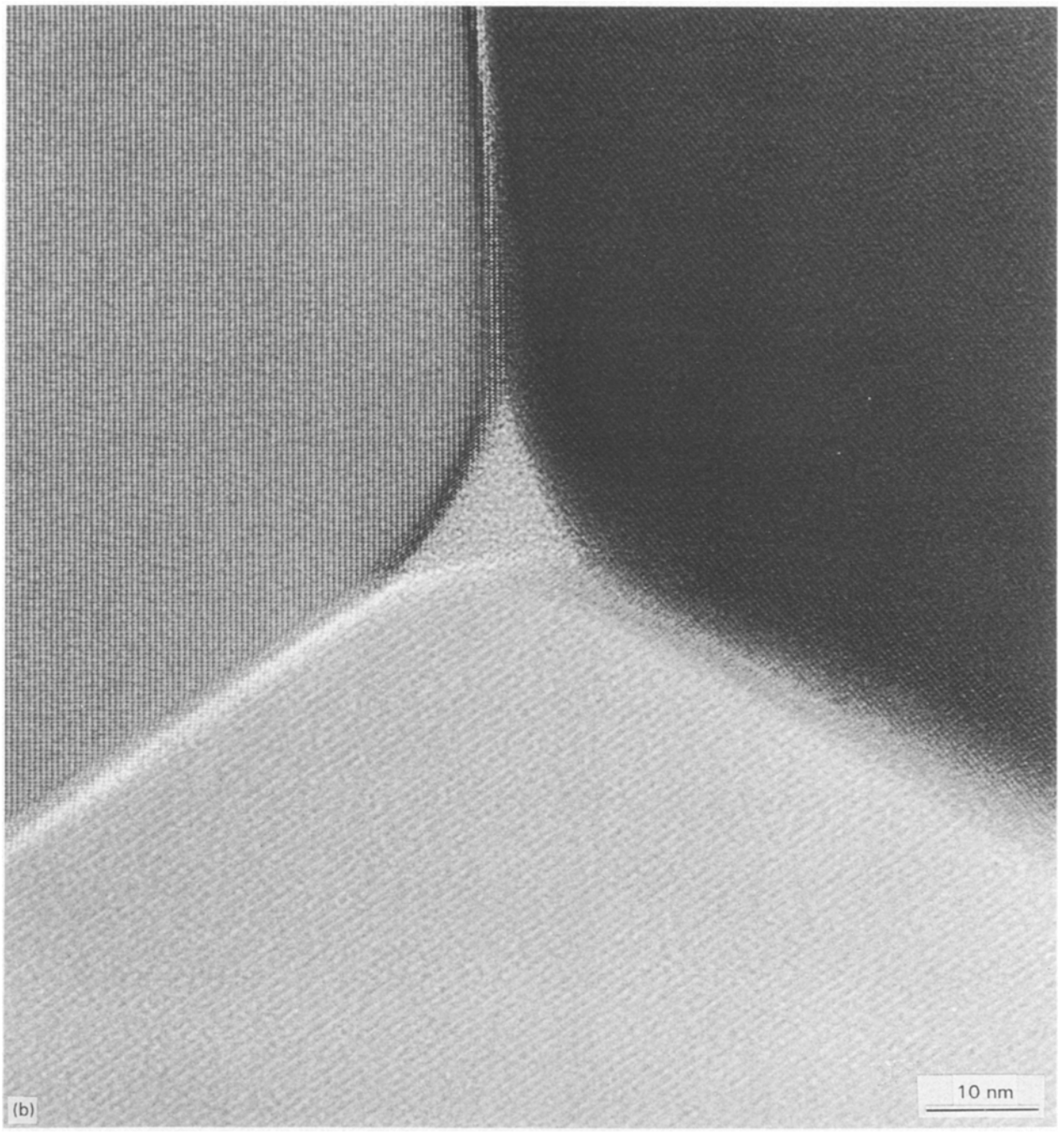

Figure 13 TEM image of (a) the Si_3N_4/Si_3N_4 interface in Composite A and (b) a triple junction between Si_3N_4 grains.

slices from the HIP-sintered specimens and then reduced to a final thickness suitable for observation by hand lapping and argon-ion etching, successively. Coating by evaporating about 5 nm carbon was performed to suppress surface charging. The first point which could be clarified concerns the status of the grain boundary after the HIP cycle. Fig. 13a shows a typical transmission electron micrograph of the Si_3N_4/Si_3N_4 grain boundary observed in Composite A. This is constituted by a thin film (average observed thickness 1 nm) of SiO_2 [13] which was present as an impurity mainly in the starting Si_3N_4 powder (cf. oxygen contents in Table I). In Fig. 13b, a triple junction of Si_3N_4 grains in the sintered body is also shown. Triple points were typically 10–20 nm in dimension and constituted by glassy SiO_2, because a clear halo-pattern was systematically found by electron diffraction.

TABLE I Impurity contents by ICP analyses on the starting powders

	O (%)	Fe (p.p.m)	Cr (p.p.m)	Ca (p.p.m)	Al (p.p.m)
Si_3N_4 powder	1.45	36	< 50	< 20	< 30
SiC Powder A	0.14	100	< 50	40	4300
SiC Powder B	0.04	220	< 500	120	50

Polytype contents of the SiC phases contained in the sintered bodies were found to be similar to that of the respective starting powders by both XRD and

Figure 14 Low-magnification TEM image of a SiC platelet showing a low density of stacking faults.

TEM analyses. The details of the determination of SiC polytypes in sintered Si_3N_4/SiC composites by XRD after a selective etching procedure, will be described in a forthcoming report [13]. Electron diffraction analyses, although performed on a very limited number of SiC platelets or particles, indicated that in the respective sintered bodies the platelets were again primarily 4H or 6H polytype, while the particles consisted mainly of 4H. The SiC phases mainly preserved their crystal structure after sintering at 2050 °C. In addition, the stacking-fault density seemed to be similar to that observed in the starting powders with the presence of relatively large unfaulted regions from a few tens of nanometres up to a few micrometres in size (Fig. 14). On the other hand, a dense array of dislocations was systemically observed inside the SiC platelets. Fig. 15a and b show the faulted structure of an SiC platelet as seen by TEM at different tilt angles. Because such faults were not observed in the starting materials, they are believed to originate during the sintering process due to the residence for long times at high temperature under the high applied pressure. A more precise characterization of the faulted structure of SiC after the present HIP sintering is presently under investigation, because it is believed that this internal structure can markedly affect the micromechanical behaviour of the reinforcing phase.

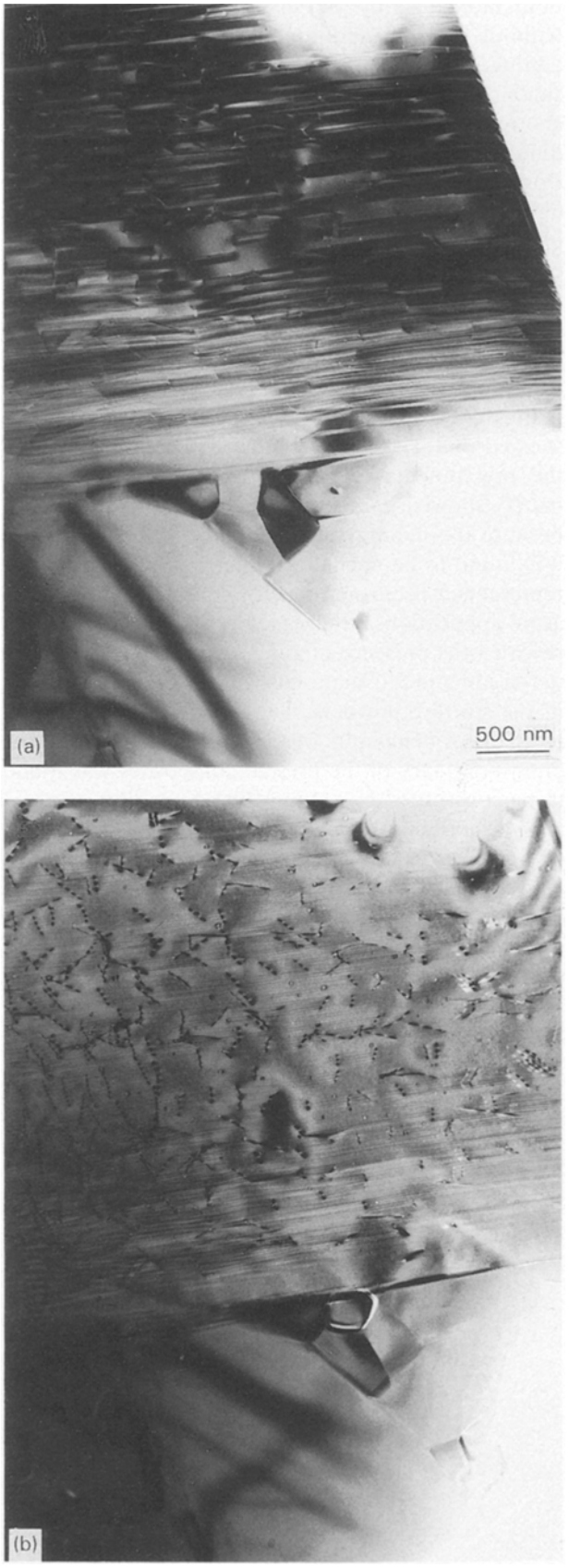

Figure 15 Planar defects in SiC platelets after sintering observed by TEM at different tilt angles.

5. Conclusion

In the present study, a characterization of the microstructure of Si_3N_4/SiC composites containing 15–40 vol % reinforcing phase has been presented. Two different composites were compared. They were

both fabricated by HIPing the same Si_3N_4 matrix without external addition of sintering aids and by adding two different SiC starting powders. Despite a similar average particle size, the two SiC raw powders showed marked crystallographic and morphological differences. A platelet-shaped powder (denominated Powder A) was found mainly constituted by 4H and 6H polytypes. However, in addition to the periodicity of the main polytypes, stacking faults were found to be ordered in such a way as to create relatively small zones of different polytypes. A lower aspect ratio powder (Powder B), having the main shape of an irregular polyhedron (histogram of number of edges in a random section closer to that of a cube), instead mainly consisted of 4H polytype. XRD analyses also showed minor amounts of the 15R polytype in both the raw powders. The SiC powders in the Si_3N_4 matrix showed good thermal stability up to 2050 °C because the main crystal structure of the SiC phase was found to be unchanged after HIP sintering. This represents a promising result for future high-temperature applications. High-resolution TEM studies also revealed the presence of a dense array of dislocations in the sintered SiC materials which were not observed in the starting powders. They may affect the micromechanical behaviour of the reinforcing phase. The grain boundary of the present composites was found to be constituted by a 1 nm thick SiO_2 film.

By examining the microstructures on a larger scale of observation, the two composites were quantitatively characterized by means of image analysis techniques. It was found that, for a similar degree of dispersion of both the materials, the three-dimensional randomness could be preserved only at $V_f < 30\%$ in the composites containing high aspect ratio platelets.

Acknowledgements

ICP analyses were performed by Messrs Y. Kohtoku and T. Nakayasu of Ube Corporation. We thank Professors T. Tadaki and S. Ueda for helpful discussions, and Professor K. Niihara for providing research facilities at the Institute of Scientific and Industrial Research, Osaka University.

References

1. I. TANAKA and G. PEZZOTTI, *J. Am. Ceram. Soc.* **75** (1992) 1023.
2. G. PEZZOTTI, I. TANAKA and T. OKAMOTO, *ibid.* **74** (1991) 326.
3. G. PEZZOTTI, *ibid.*, **76** (1993) 1313.
4. G. PEZZOTTI, B.-T. LEE, T. NISHIDA and K. HIRAGA, *J. Mater. Sci.* submitted.
5. J. F. HILLIARD, Report 62-RL-3133M, General Electric Research Laboratories, Schenectady, NY, December 1962.
6. I. TANAKA, G. PEZZOTTI, T. OKAMOTO, Y. MIYAMOTO and M. KOIZUMI, *J. Am. Ceram. Soc.* **72** (1989) 1656.
7. F. C. HULL and W. J. HOUK, *Trans. AIME* **197** (1953) 565.
8. R. L. FULLMAN, *ibid.* **197** (1953) 447.
9. E. E. UNDERWOOD, in "Quantitative Stereology" (Addison-Wesley, MA, 1970) pp. 58, 83, 92.
10. J. E. HILLIARD and J. W. CAHN, *Trans. AIME* **221** (1961) 344.
11. J. E. HILLIARD, Report 61-RL-2652M, General Electric Research Laboratories, Schenectady, NY, March 1961.
12. S. A. SALTYKOV, in "Stereometric Metallography" (Metallurgizdat, Moscow, 1958).
13. I. TANAKA, G. PEZZOTTI, K. MATSUSHITA, Y. MIYAMOTO and T. OKAMOTO, *J. Am. Ceram. Soc.* **74** (1991) 752.
14. G. PEZZOTTI, T. NISHIDA, K. NIIHARA and S. UEDA, *J. Mater. Sci.*, to be published.

Received 3 November 1992
and accepted 11 January 1993